

1.55 μm Bipolar Cascade Segmented Ridge Lasers

Jonathan T. Getty, Leif A. Johansson, Erik J. Skogen, and Larry A. Coldren, *Fellow, IEEE*

Abstract—Scalable bipolar cascade lasers are achieved by electrically segmenting an InP ridge laser, and then series-connecting the segments.

Lasers with up to 12 stages are demonstrated with record 390% continuous wave differential efficiency, and very low threshold currents. Three-stage lasers with 50 Ω input impedance and over 100% differential efficiency are modulated with 2.5 GB/s digital data, and have 5 GHz analog modulation bandwidth. Noise and distortion properties are at least as good as single-stage control lasers.

Index Terms—Bipolar cascade lasers, impedance matching, integrated optoelectronics, ion implantation, optical amplifiers, quantum well (QW) intermixing, semiconductor lasers.

I. INTRODUCTION

CONVENTIONAL semiconductor lasers are less than perfectly suited to efficient radio frequency (RF) direct modulation. A differential quantum efficiency (DQE, the ratio of photons emitted in the laser mode to electrons in the drive current [1]) below unity guarantees that the signal will diminish on transmission, requiring amplification to provide signal gain and degrading the noise performance of the optical link. The low resistance of a forward-biased diode matches poorly to a 50 Ω RF source, and worse to a higher impedance integrated photodiode. When specifications require a broadband impedance match, series-connected resistors drain RF power from the source, further reducing the modulation efficiency.

Bipolar cascade lasers or laser arrays have traditionally been proposed [2] to address both the low DQE and input impedance of simple diode laser. In principle, the bias and modulation currents are driven, in series, through multiple diodes, each one contributing both photons and resistance. This multiplies the limit on DQE to 100% per diode, and increases the resistance proportionally (sublinearly, linearly, or quadratically, depending on the type of cascade laser). But, in practice, cascade lasers have been limited to a modest number of stages, and excess optical loss has limited DQE to just over 100%, hardly high enough to justify the added complication in growth and processing.

Most of the prior work [3]–[7] on cascade lasers has focused on vertically stacked structures, in which multiple active regions are grown, alternated with thin, highly doped Esaki junctions [3]–[5]. The current is inserted at the top of the diode stack, and recombines in each active region before tunneling to the next, while light can be emitted from the edge or surface. This method shows promise for increasing gain in long wavelength VCSEL (Vertical Cavity Surface Emitting-Laser) structures, but

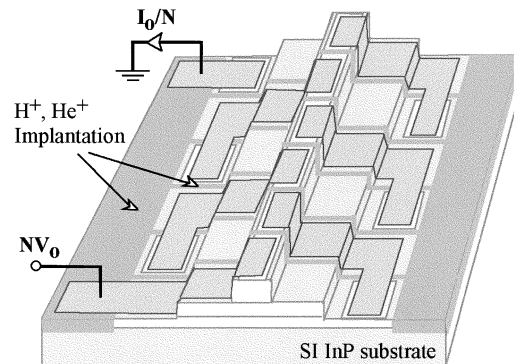


Fig. 1. Three-dimensional schematic of bipolar cascade segmented ridge laser. The dark grey areas are ion-implanted to force current, in series, through N diode stages.

most published work has been limited to 3–4 stages by heating and epitaxial constraints, reaching 130% DQE in recent publications [5]. Higher efficiencies can be achieved by series-connecting a laser array [8], [9], but coherent combination of even a modest number of beams is difficult at best, resulting in large coupling losses when anything besides a large-area photodetector is employed. As a result of this limited scaling, bipolar cascade lasers to date have yet to improve significantly enough upon the DQE of single-stage lasers to justify the increased complexity.

This paper, therefore, employs the segmented laser structure shown in Fig. 1, because it is scalable to an arbitrarily large number of stages, limited only by voltage constraints, the narrow width of the electrically dead region between stages, and optical loss introduced in these regions. A standard laser ridge waveguide is etched as shown, ion implantation divides the laser into N electrically isolated regions, and metal interconnects are formed to contact the semiconductor and connect adjacent stages. Current is driven into the p-doped ridge of the first stage, generates electrons and holes, which recombine in the active region, and exits the semiconductor through the topside n-contact at lower right. The same current then reenters the ridge of the second stage, again generates electrons and holes in the second diode, and similarly continues through the series-connected chain of N diodes, and exits at the ground contact at upper left.

II. THEORY

An understanding of the behavior of such a multistage laser can be had by comparison with a single-stage control laser of length L and ridge width w , threshold current I_1 and DQE η_1 [1]. The control laser has some total (internal and mirror) loss α_1 , and reaches threshold when its current density $J_1 = I_1/wL$

Manuscript received February 15, 2003; revised July 23, 2003.

The authors are with the Electrical and Computer Engineering Department, University of California at Santa Barbara, Santa Barbara, CA 93106 USA (e-mail: jtg0@umail.ucsb.edu).

Digital Object Identifier 10.1109/JSTQE.2003.819482

produces sufficient gain to offset these losses. The N -stage cascade laser has an excess “segmentation” loss α_{seg} due to scattering or absorption between stages, totaling

$$\alpha_N = \alpha_1 + (N - 1)\alpha_{\text{seg}}. \quad (1)$$

If we neglect the width of the implanted stripe between sections, assume a logarithmic gain model $g(J) = g_0 \ln(J/J_{\text{tr}})$, and solve for the threshold conditions (I_N, J_N) of an otherwise identical N -stage laser

$$\begin{aligned} J_N &= J_{\text{tr}} \exp(\alpha_N/\Gamma g_0) \\ &= J_{\text{tr}} \exp[(\alpha_1 + (N - 1)\alpha_{\text{seg}})/\Gamma g_0] \end{aligned} \quad (2)$$

$$J_N = J_1 \exp[(N - 1)\alpha_{\text{seg}}/\Gamma g_0] \quad (3)$$

$$J_N \approx J_1 + J_1[(N - 1)\alpha_{\text{seg}}/\Gamma g_0]. \quad (4)$$

This current density is achieved by driving a current through N stages of length L/N

$$I_N = J_N w(L/N) \quad (5)$$

$$I_N = (J_1 w L/N) + [(N - 1)J_1 w L \alpha_{\text{seg}}/N \Gamma g_0] \quad (6)$$

$$I_N \equiv (I_1/N) + I_0[(N - 1)/N]. \quad (7)$$

For the lasers presented in this paper, $I_0 < 0.50$ mA, and the threshold current scales as (roughly) inversely proportional to the number of stages, *because the same current density is achieved with N times less current*. Similarly, above threshold, a given current density is provided by N times less terminal current. Since injection efficiency η_i and mirror loss α_m are independent of the number of stages

$$\eta_1 = \eta_i \alpha_m / \alpha_1 \quad \eta_N = N \eta_i \alpha_m / \alpha_N \quad (8)$$

$$\eta_N = N \eta_1 \alpha_1 / \alpha_N \quad (9)$$

and differential efficiency increases linearly with the number of stages as long as the segmentation loss is kept low.

To summarize thus far, the DQE of a cascaded segmented ridge laser increases linearly with the number of stages, while the threshold current decreases as $1/N$. Both effects saturate at large N due to segmentation loss, and are compensated with higher voltage and impedance through the diode chain. Voltage increases linearly with the number of stages, but the voltage per stage decreases slightly as the stages became shorter, due to more uniform distribution of current in each stage. Input impedance increases not only because of the number of series-connected stages, but also because those stages become smaller as a laser of fixed length is subdivided; it scales by N^2 if the laser length is fixed, and by N if the stage length is fixed.

III. DEVICE AND FABRICATION

We have now described a laser with enhanced differential efficiency and input impedance; the difficulty lies in preventing current leakage between stages, and keeping the segmentation loss low enough to make a large number of stages worthwhile. Doing so requires a method which provides at least 100 k Ω leakage path isolation between adjacent diode stages, is compact

(since such isolation regions are inherently passive), and introduces as little segmentation loss as possible. Some past work [6] has isolated stages by etching away the waveguide cladding in a narrow section, but this perturbs the waveguide and introduces a fatal amount of optical scattering. Instead, we have used H^+ and He^+ ion implantation to kill conductivity in the p- and n-type InP, respectively. A 3- μm stripe is implanted through to the semi-insulating substrate, providing more than 1 M Ω of interstage isolation without disturbing the optical mode.

Unfortunately, this creates another problem. Leakage conductivity must be eliminated both in and under the active region of the waveguide, which is exposed to a moderate dose of He^+ implantation. As in the bulk InP regions, the implantation damage disrupts the lattice, greatly reducing the carrier lifetime, preventing conduction, but also preventing a stable population inversion. Photons enter the implanted active material, and are quickly absorbed; the electron and hole pair immediately recombine nonradiatively, and the optical absorption cannot be bleached. A single 3- μm implant stripe can absorb about 40% per pass, making lasing, not to mention efficient segmentation, unlikely.

To correct this problem, two alternatives were considered. The first was to grow offset quantum wells (QWs) on top of the waveguide, etch the QWs from the areas to be implanted, and regrow a p-InP cap. This fairly straightforward approach has two flaws: first, replacing the high-index QWs with InP perturbs the optical mode, causing $\alpha_{\text{seg}} > 0.13$ dB/pass (etch roughness increased this number in actual devices to 0.3–0.5 dB); second, growing the QWs on the top of the waveguide reduces their overlap with the optical mode, increasing the threshold current, and reducing continuous wave (CW) output power (lasers fabricated by this method lased pulsed, but not CW, mostly due to a poor n-contact layer). The second, and more successful, option was to grow a centered, multiple QW (MQW) active region and passivate it in area of the He^+ implant.

Many QW intermixing techniques [10]–[12] can locally blueshift the absorption edge beyond the lasing wavelength, but the process must be well confined to the desired area, stable, reliable, and have little effect on the unshifted material. To this end, we have developed a novel ion implantation-induced QW intermixing (IIQWI) method which uses an undoped, sacrificial layer as a medium for the intermixing process (more fully described in [11]). We modify the conventional method pioneered by Charbonneau [12], by growing a 4500 Å undoped InP layer atop the waveguide. Regions to be blueshifted are implanted with low-energy (100 keV) P^+ to create point defects near the surface, which are driven through the underlying QWs by a 690 °C rapid thermal anneal (RTA). The resulting vacancies enhance the natural intermixing of QW and barrier atoms that occurs at high temperatures, with the effects shown in Fig. 2. The undoped layer is then removed, taking the source of the dislocations with it, and a p-InP cap is regrown. This method offers several improvements over the conventional method of implanting a fully grown epitaxial structure. The thinner InP layer reduces anneal temperatures, better localizing the blueshift (to $< 2 \mu\text{m}$ from the implant), reducing the effects on unimplanted areas, and decreasing the chance of surface damage during the anneal; the elimination of the implanted

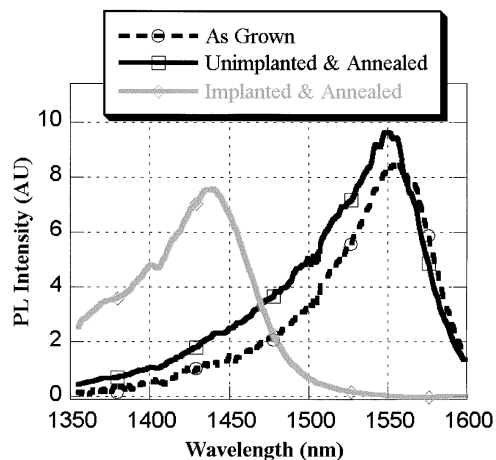


Fig. 2. Effect of QWI process on implanted and unimplanted material. Segmentation loss comes from the tail of the implanted and annealed material overlapping the lasing wavelength.

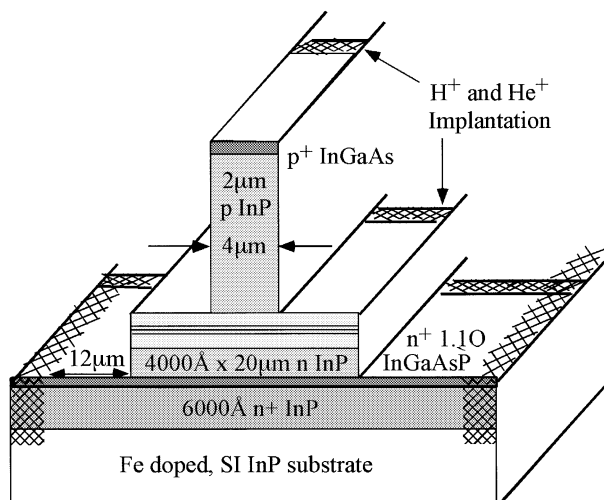


Fig. 3. Laser ridge cross section showing epitaxial structure and geometry. N-contacts are formed on the n^+ InGaAsP layer. Implanted areas are shown in crosshatch.

material stabilizes the effect during further processing; and the absence of Zn during the process prevents it from diffusing into the QWs and increasing loss throughout the laser.

Once QWs in the isolation regions have been intermixed, and the sample regrown, the laser ridge is etched as shown in Fig. 3. An n^+ InGaAsP layer is exposed, and Ni/AuGe/Ni/Au n-contacts are deposited and annealed. At this point, the isolation implantations are performed, implanting a $3\text{-}\mu\text{m}$ stripe, centered on a $6\text{-}\mu\text{m}$ intermixed region, between each laser stage. SiN_x is deposited on the samples, and p-contact vias are opened, before Ti/Pt/Au is evaporated and annealed as seen in Fig. 4, forming both p-contacts and interconnects between adjacent stages. Finally, the sample is thinned, cleaved, and individual laser bars are soldered to AlN carriers to improve heatsinking. To simplify analysis, all lasers presented in this work were tested on a 20°C temperature-controlled stage, and the facets left uncoated.

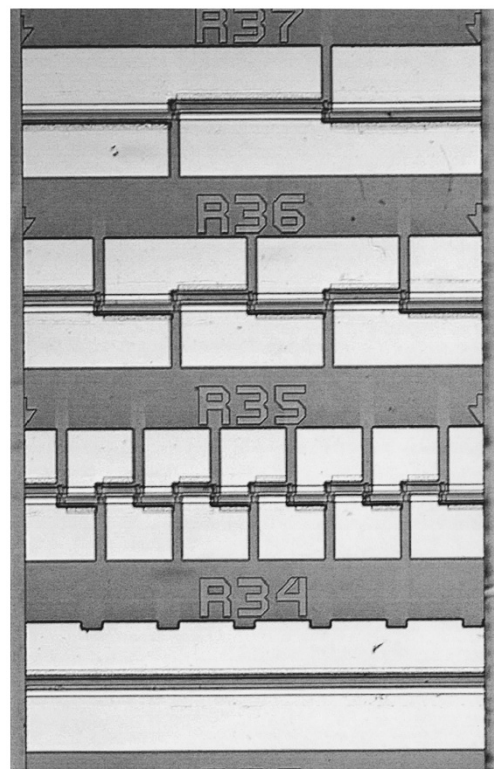


Fig. 4. Micrograph of a typical $600\text{-}\mu\text{m}$ laser bar. The laser on the left (R34) is a single-stage control laser. To its right are 12-stage (R35), six-stage (R36), and three-stage (R37) cascade lasers. The laser ridge itself is centered between each set of contacts.

IV. RESULTS

In analyzing any novel laser with “world record” properties, it is important to ask not just how low or how high it goes, but whether its other properties make it a practical device. We will endeavor to show that not only does the segmented laser improve differential efficiency, threshold current, and matching, it also operates with good CW power, modulates efficiently at high speed, and with low noise and distortion. In most cases, these comparisons are made with the single-stage control laser fabricated alongside the multistage lasers (as in Fig. 4). While these control lasers may not be state of the art themselves, they serve to measure whether the segmentation and cascading of the multistage lasers deteriorates their performance.

A. Scaling

Fig. 4 shows, from left, a $600\text{-}\mu\text{m}$ control laser, and 12-, six-, and three-stage laser (of $50\text{-}\mu\text{m}$, $100\text{-}\mu\text{m}$, and $200\text{-}\mu\text{m}$ stages, respectively). Laser sets of this type were tested by sweeping the laser bias and detecting the emission from one facet with an integrating sphere. The dramatic CW results are shown in Fig. 5, and tabulated in Table I. The differential efficiency scales slightly sublinearly with the number of stages, increasing steadily to 390% at 12 stages, an 11-fold improvement over the control laser. Threshold current falls as the number of stages increase, with the 12-stage threshold reduced by more than a factor of ten, to 2.74 mA. All of the lasers are quite robust, and emit up to 20 mW per facet, with a multimode spectrum centered at $1.55\text{-}\mu\text{m}$, as shown in Fig. 6.

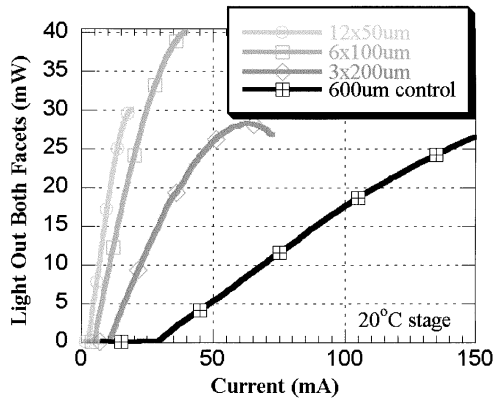


Fig. 5. CW L-I response of a 600 μm laser, subdivided into 1, 3, 6, and 12 stages. DQE exceeds 100% in all but the control laser.

TABLE I
ROOM TEMPERATURE, CW
CHARACTERISTICS OF THE CONTROL
AND SEGMENTED LASERS SHOWN IN FIG. 5

Stages & Length	Differential Efficiency	Threshold Current	Threshold Voltage	DC Input Impedance
12x50 μm	390%	2.74 mA	11.3 V	471 Ω
6x100 μm	218%	4.77 mA	5.8 V	117 Ω
3x200 μm	126%	10.4 mA	3.0 V	48 Ω
1x600 μm	34%	28mA	1.05 V	5.5 Ω

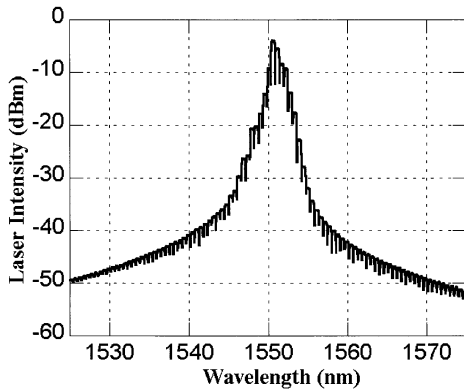


Fig. 6. Optical CW spectrum of a typical six-stage laser, 10 mA above threshold. The multimode behavior is typical of Fabry-Perot lasers, and the mode spacing corresponds to the cavity length.

Such improvements must be “paid for,” and the voltage increases with the number of stages. However, due to the more uniform current density of shorter stages, the voltage per stage drops from 1.05 V in the control laser to 0.94 V in the 12-stage device, ensuring that the threshold power is roughly constant with the number of stages. Resistance scales roughly quadratically with the number of stages, reaching 50 Ω for the three-stage laser (which will be discussed at length later), which itself has a differential efficiency greater than unity.

In practice, the scaling of cascade lasers is limited by the large voltage and impedance of very long diode chains, as well as the finite length of the isolation region between stages, and its optical absorption. However, scaling of the present generation

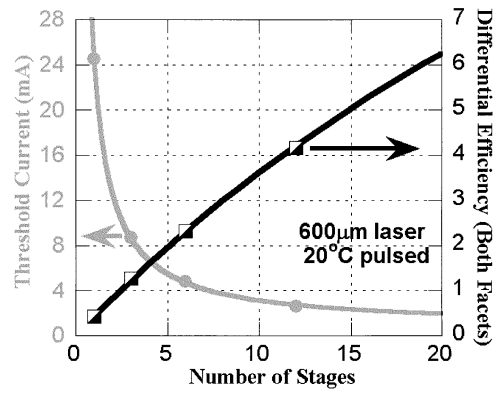


Fig. 7. Calculations of threshold current and DQE [as given in (7) and (8)] for 600- μm lasers, overlaid with experimental pulsed data. The simulations fit $I_1 = 24.5$ mA, $I_0 = 0.47$ mA, $\alpha_{\text{seg}} = 0.15$ dB/pass, $\eta_i = 0.694$, and $\alpha_1 = 12.2$ cm^{-1} .

of devices was limited by the shortest stage length (50 μm) included on the mask, so longer lasers with up to 19 stages were tested, and lased CW with over 500% DQE, 2.1 mA, 19.0 V threshold, and 930 Ω input impedance.

B. Analysis

The success of these lasers is owed mostly to the extremely low loss of the implanted, intermixed region between stages. The curve fits in Fig. 7 model the scaling of threshold current and differential efficiency and find a segmentation loss of 0.15 dB/pass, an outstanding result due to the large relative blueshift shown in Fig. 2. Further, the QWI process has not seriously degraded the control lasers, which exhibited an injection efficiency of 69.4% injection efficiency, with an internal loss of 12.2 cm^{-1} in a seven-QW active region. Lasers made with the conventional intermixing process (which exposes the active region to Zn diffusion) had at least 20 cm^{-1} internal loss when the sample was annealed hot enough to achieve the desired blueshift.

Two areas of potential improvement would reduce the threshold currents considerably. The laser ridge was 4.2- μm wide, almost twice the optimal amount, due to a conservative process and the imprecision of contact alignment. Also, analysis of the gain curve of the laser material indicates a transparency current density of 87 A/cm² per well, much higher than that achieved by similar active regions on conducting substrates. This is reflected in nonintermixed broad-area lasers from the same growth, and will require further optimization of the epitaxy.

C. 50 Ω Lasers

In RF electronics, it is usually desirable to match the input impedance of a load to the 50 Ω source impedance of the network, to eliminate mismatch reflections and ensure maximum power transfer [13]. Where a laser is involved, it should be noted that the latter is not always the case. The output power of a laser is determined by its current (which is twice as high for a short as for a 50 Ω match), not its electrical input power, and reflections can be managed when the laser driver is integrated [14]. However, in practice, system requirements often insist that low-impedance lasers be matched to 50 Ω by adding a

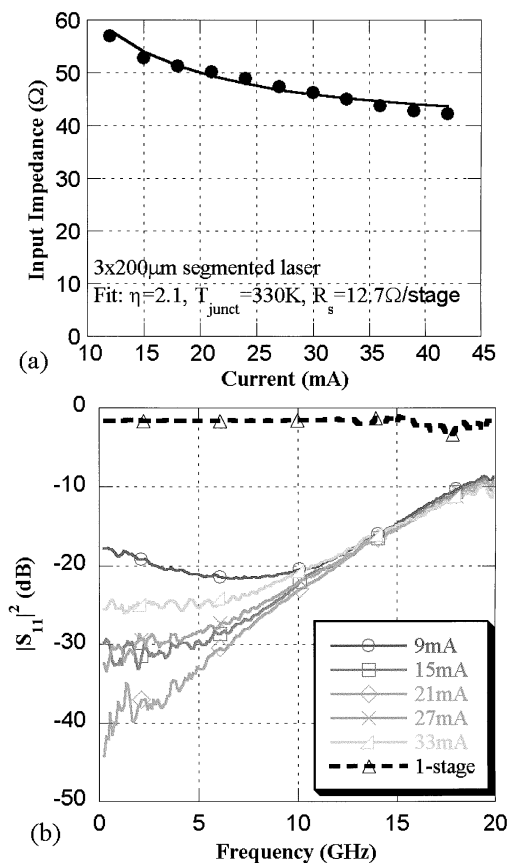


Fig. 8. Input impedance of the three-stage laser drops with current as dV/dI of the diode is reduced. (a) Impedance at low frequencies, extracted from S-parameter measurements, as shown in (b). Also note the poor S_{11} of the control laser.

series-connected resistor. This complicates packaging and integration, adds a considerable heat source to the package, and requires a higher voltage driver to compensate.

In contrast, a multistage laser achieves a higher input impedance by series connecting laser stages, and recycling the current. This means that, while a three-stage laser and resistor-matched conventional laser draw the same RF current, the modulating current density in the three-stage laser is three times higher, and the light modulation output is three times greater. If the impedance of the system is greater than $50\ \Omega$ (perhaps $100\ \Omega$ or a high-impedance photodiode), the segmented laser offers a proportionally greater improvement over a single-stage laser.

The input impedance of a laser is equal to the slope dV/dI at the laser's bias point, and changes with bias, so it is critical that the laser be well matched near its bias point. Fig. 8(a) confirms the matched, low-frequency impedance of a three-stage laser, extracted from the electrical S_{11} parameter in Fig. 8(b). The laser reaches $50\ \Omega$ at 21 mA (optimal digital transmission bias = 20.5 mA), and rolls off at higher frequency due to the capacitance of the large probing pads seen in Fig. 4.

D. High-Speed Operation

It is a reasonable concern that the complex current path of a bipolar cascade laser might compromise its high-speed perfor-

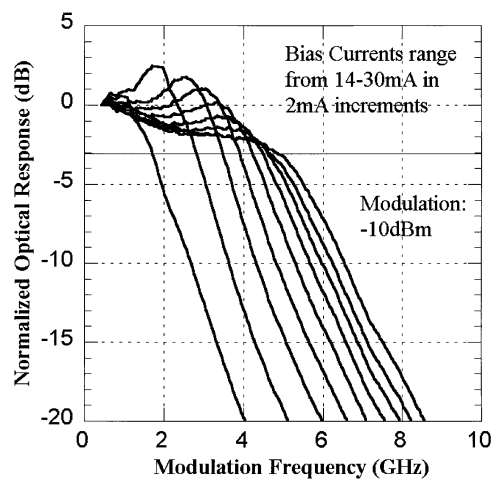


Fig. 9. Analog bandwidth measurement of a three-stage laser. Three-dB bandwidth increases with power (see Fig. 10), and achieves a maximum of 5 GHz at 30 mA bias.

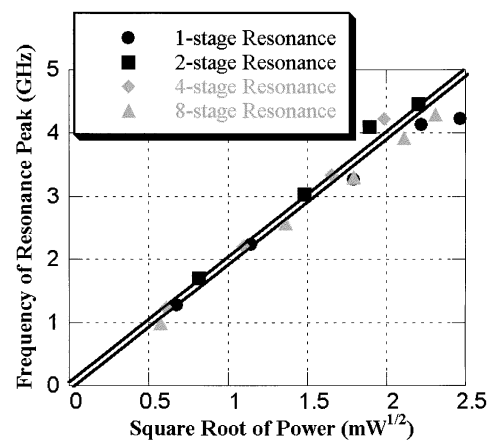


Fig. 10. Frequency of the resonance peak increases as the square root of power, but does not depend on the number of stages. This and Fig. 12 use $400\text{-}\mu\text{m}$ lasers because they were compatible with available high-speed probes.

mance. Modulation bandwidth might be limited by charge transport delays, unforeseen resonances in “abnormal” rate equations [9], or excess capacitance, as noted above. To test this, a matched three-stage laser was directly contacted with a 40-GHz ground-signal probe, and connected through a bias tee to a network analyzer, as used for the S_{11} measurement above. The laser was then separately direct current (DC)-biased, and a $-10\ \text{dBm}$ RF signal was frequency swept and detected by a lensed fiber, with results shown in Fig. 9.

The bandwidth increases with bias as the square root of optical power, and is governed by the relaxation resonance of the laser, the same mechanism that limits the speed of conventional diode lasers. To determine whether the cascaded laser is in some way inferior to a conventional laser, we observed the resonance peaks of multistage and control lasers at increasing bias. Fig. 10 shows that not only do both multistage and control lasers follow a $f \sim P^{1/2}$ dependence, but this dependence is invariant with the number of stages. The resonance peaks shown in Fig. 10 must be extrapolated (at higher powers, the peak flattens and cannot be accurately determined), but demonstrate a potential for resonance frequencies as high as 6–7 GHz, perhaps reaching

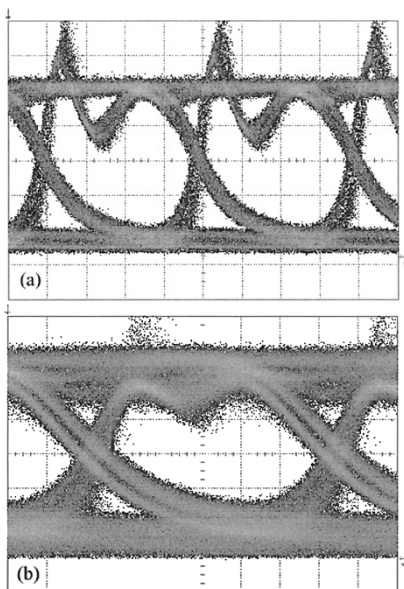


Fig. 11. Unfiltered eye diagrams for (a) three-stage and (b) control lasers. The three-stage laser is biased at 20.5 mA with 1.0 V_{p-p} modulation, and has a 9.6-dB extinction ratio. The control laser is biased at 63 mA with 2.0 V_{p-p} modulation, and has a 8.0-dB extinction ratio.

10 GHz if a thinner laser ridge were used, increasing the photon density and bandwidth.

Digital data transmission is a fair test of any purported high-speed laser. Unlike the small-signal, single-frequency modulation used to measure analog bandwidth, digital data modulates with a large signal and considerable harmonics, to maximize the on-off extinction ratio and bit-error rate. Single-stage control and three-stage cascade lasers were probed as described for analog measurements, biased, and driven with a 2.5-Gb/s pattern generator with adjustable output. DC bias current and digital power were optimized for maximum extinction ratio, and a clean, unfiltered eye pattern, as shown in Fig. 11. The three-stage laser [Fig. 11(a)] achieves a 9–10-dB extinction ratio with a 20.5 mA bias, and 0.9 V_{p-p} digital input signal. The control laser [Fig. 11(b)], however, biased at 63 mA, manages only an 8-dB extinction ratio with a degraded eye, at the maximum digital input signal of 2 V_{p-p} .

The superior performance of the three-stage laser is ascribed to the poor matching between the 50- Ω digital source and the 6- Ω control laser, resulting in poor power delivery to the laser, such that the maximum output of the pattern generator was insufficient to reach the optimal signal level. This demonstrates a major advantage of the segmented laser. Although a larger DC voltage is required to turn it on, a much smaller RF signal is required to modulate it. In applications with a 50 Ω or greater (e.g., photodiode) integrated drive circuit, this means that a multistage laser will require less voltage and less current than a conventional laser.

E. Noise and Distortion

A high-speed analog or digital directly modulated link requires more than sufficient bandwidth. The optical output from the laser must have low in-band noise and distortion to be useful in an actual RF link, and it remains to be shown that such ef-

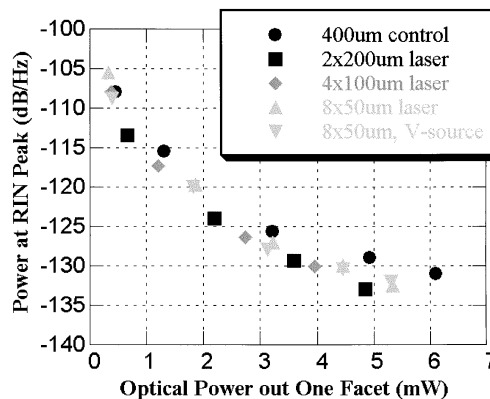


Fig. 12. RIN peak intensity is plotted against optical power, and does not show a strong dependence on the number of stages, or the biasing method.

fects are not enhanced in a bipolar cascade laser. A common handwaving argument holds that since spontaneous emission is determined by threshold current (which is reduced by $1/N$ in a segmented laser), noise should improve by a factor of N over a conventional laser. This is false because the N -stage laser operates at the same (or slightly higher) current density, giving rise to the same spontaneous emission level at threshold. Alternatively, Rana and Ram have demonstrated that positive noise correlation between discrete series-connected lasers did occur when the lasers were biased with a low-impedance voltage source, but not with a high-impedance current source [8]. In our experiments, the lasers were biased with a variety of power supplies in both current and voltage source modes. Both yielded the same results, showing no noise enhancement, but perhaps indicating the necessary probe configuration creates a high source impedance at the GHz frequencies in question.

Relative intensity noise (RIN) is measured by DC biasing the laser and illuminating a 12-GHz photodetector, then amplifying and displaying the detected signal on a spectrum analyzer. Thermal, dark current, and shot noise are subtracted from the noise spectrum, leaving only those contributions due to the laser kinetics. These RIN spectra show a peak at the resonance frequency of the laser, the intensity of which drops as the power and frequency increase. Four lasers, with one, two, four, and eight stages, adjacent on the same 400- μm -long laser bar, were tested, and the intensity of these peaks is plotted against peak frequency in Fig. 12. Although there is some scatter in the data, there is no appreciable noise enhancement or reduction caused by dividing the laser into series-connected stages, or biasing with a voltage supply.

Distortion is a concern when multiple RF frequencies directly modulate a laser simultaneously. Nonlinearities in the modulation response mix these frequencies, transferring power to sum and difference frequencies throughout the RF band. Of particular concern are the third-order harmonics of frequency $f_3 = 2f_1 - f_2$; where f_1 and f_2 are similar modulation frequencies (499 and 501 MHz in these experiments). While even-order harmonics such as $f_1 \pm f_2$ are usually out of band and easily filtered, third-order harmonics project back into the modulation band, and are difficult or impossible to remove. For this reason, the directly modulated laser needs to be very linear and produce as little distortion as possible.

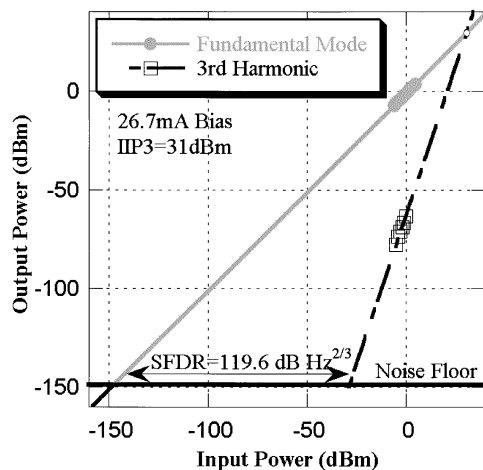


Fig. 13. Distortion measurement on a three-stage laser. IIP3 marks the input power at which the fundamental and third harmonic extrapolations cross.

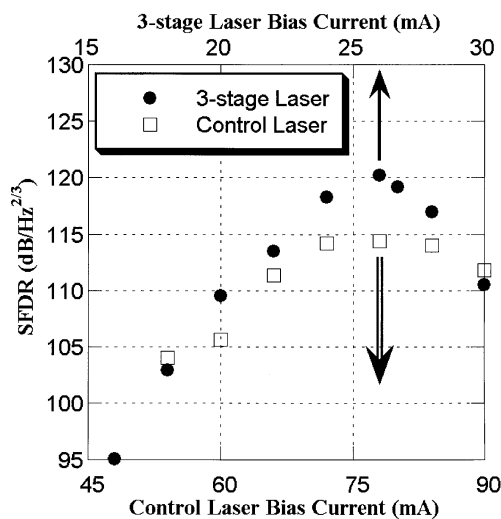


Fig. 14. SFDR for 600- μm control and three-stage lasers. The x-axes are aligned to correspond to the same current density.

Spurious-free dynamic range (SFDR) is a common measurement of distortion, and measures the difference in input power between the points at which the fundamental and third-order distortion peaks cross the 1-Hz noise floor. Two RF modulations tones, f_1 and f_2 , at an equal, variable power, are injected into the laser through the RF port of a bias tee. As usual, the laser is independently biased by a current source through the DC port. The light is detected, the electrical signal amplified, examined on a spectrum analyzer, and plotted at varied RF input power, as for the three-stage laser in Fig. 13. The receiving circuit raises the noise floor, so the received power at f_1 and $2f_1 - f_2$ are extrapolated back to the laser's noise floor, and SFDR measured. SFDR varies with bias as shown for three-stage and control lasers in Fig. 14, but for equal optical power levels, there is no added distortion in the multistage laser. The lower SFDR of the control laser is caused mainly by higher RIN.

V. CONCLUSION

We have, for the first time ever, fabricated bipolar cascade lasers that scale viably to a large number of stages, and demonstrated record differential efficiencies well beyond unity, 50- Ω matched lasers with enhanced, instead of reduced, modulation response, and up to 40 mW of CW output power at 1.55 μm . Further, the fabrication process is compatible with single-regrowth active-passive and widely tunable lasers, and can be used to provide gain in integrated photonic circuits. We then demonstrated that the multistage lasers are equal to or better than conventional lasers in terms of analog and digital bandwidth, modulation efficiency, noise, and distortion. There are no booby traps associated with the bipolar cascade segmented ridge laser.

These hurdles cleared, a number of integration projects lie ahead. The segmented laser can be used as an active region between two tunable mirrors, to create a tunable laser with positive gain. Driven by a photodetector, this cascaded tunable laser can form a lossless tap, or an amplifying wavelength converter. Further, a matched laser makes integration easier by eliminating meander-line resistors that would otherwise consume space and power while heating the chip. In short, these lasers can be tailored to a desired gain, impedance, threshold current, and voltage, a valuable advantage in the growing world of photonic integrated circuits.

REFERENCES

- [1] L. A. Coldren and S. W. Corzine, *Diode Lasers and Photonic Integrated Circuits*. New York, NY: Wiley, 1995.
- [2] H. Yuen, "Amplification of quantum states and noiseless photon amplifiers," *Phys. Lett.*, vol. 113A, no. 8, pp. 405–407, 1986.
- [3] W. Schmid *et al.*, "CW operation of a diode cascade InGaAs quantum well VCSEL," *Electron. Lett.*, vol. 34, pp. 553–555, 1998.
- [4] J. Kim *et al.*, "Near-room-temperature CW operation of electrically pumped, multiple-active-region 1.55 μm VCSEL's with high differential efficiency," *Appl. Phys. Lett.*, vol. 77, pp. 3137–3139, 2000.
- [5] T. Knodl, M. Golling, A. Straub, and K. J. Ebeling, "Multi-diode cascade VCSEL with 130% differential quantum efficiency at CW room temperature operation," *Electron. Lett.*, vol. 37, pp. 31–33, 2001.
- [6] J. T. Getty *et al.*, "Monolithic, series-connected segmented-ridge lasers," *Electron. Lett.*, vol. 35, pp. 1257–1258, 1999.
- [7] S. G. Ayling *et al.*, "Intrinsically matched 50 ohm laser arrays with greater than 100% quantum efficiencies for optically coupled transistors and low-loss fiber optic links," in *Proc. SPIE Photonics West: Laser Diode Applications IV*, 1998. Paper 36.
- [8] F. Rana and R. J. Ram, "Current noise and photon noise in quantum cascade lasers," *Phys. Rev. B, Condens. Matter*, vol. 65, no. 12, pp. 125313/1–125313/29, Mar. 15, 2002.
- [9] K. D. Choquette and E. Young, "Cascade vertical cavity surface emitting laser arrays," presented at the *LEOS 2002 Annu. Meeting*, Glasgow, U.K., 2002. Paper TuAA1.
- [10] S. K. Si, D. H. Yeo, K. H. Yoon, and S. J. Kim, "Area selectivity of InGaAsP-InP multi-quantum-well intermixing by impurity-free vacancy diffusion," *IEEE J. Select. Topics Quantum Electron.*, vol. 4, pp. 619–623, July-Aug. 1998.
- [11] E. J. Skogen *et al.*, "A quantum-well intermixing process for wavelength-agile photonic integrated circuits," *IEEE J. Select. Topics Quantum Electron.*, vol. 8, pp. 863–869, July-Aug. 2002.
- [12] S. Charbonneau *et al.*, "Quantum-well intermixing for optoelectronic integration using high energy ion implantation," *J. Appl. Phys.*, vol. 78, pp. 3697–3705, 1995.
- [13] D. K. Cheng, *Field and Wave Electromagnetics*. New York: Addison-Wesley, 1989.

- [14] R. J. Ram *et al.*, "Cascade semiconductor lasers for telecommunications," presented at the *LEOS 2002 Annu. Meeting*, Glasgow, U.K., 2002. Paper WV3.

Jonathan T. Getty was born in Princeton, NJ, in 1974. He received the B.S. degree in electrical engineering from Cornell University, Ithaca, NY, and the M.S. and Ph.D. degrees from the University of California, Santa Barbara, both in electrical and computer engineering, in 1998 and 2003, respectively.

Between his undergraduate and graduate studies, he worked on satellite transponders at the Jet Propulsion Laboratory, Pasadena, CA. His current research interests include design, fabrication, and characterization of bipolar cascade and conventional semiconductor lasers, photonic integrated circuits, and ion implantation for electrical isolation and quantum-well intermixing.

Leif A. Johansson received the M.Sc. degree from the Royal Institute of Technology (KTH), Stockholm, Sweden, in 1997, and the Ph.D. degree from University College London (UCL), London, U.K., in 2002.

His research interests at UCL included generation and transmission of millimeter-wave modulated optical signals, millimeter-wave modulated analog optical links, fiber-radio systems, and feed-forward linearization of directly modulated lasers. In 2002, he joined the University of California, Santa Barbara, as a Postdoctoral Researcher. His current research interests include design and characterization of integrated photonic devices for analog and digital applications.

Erik J. Skogen was born in Minneapolis, MN, in 1975. He received the B.S. degree from Iowa State University, Ames, in 1997, and the M.S. degree in 1999 from the University of California, Santa Barbara, where he is currently working toward the Ph.D. degree in electrical and computer engineering.

His current research interests include widely tunable semiconductor lasers, monolithic integration for photonic integrated circuits, growth aspects in the InGaAsP material system using MOCVD, and quantum-well intermixing.

Larry A. Coldren (S'67-M'72-SM'77-F'82) received the Ph.D. degree in electrical engineering from Stanford University, Stanford, CA, in 1972.

After 13 years in the research area at Bell Laboratories, he was appointed Professor of Electrical and Computer Engineering at the University of California, Santa Barbara (UCSB), campus in 1984. In 1986, he assumed a joint appointment with Materials and ECE, and in 2000 the Fred Kavli Chair in Optoelectronics and Sensors. He is also Chairman and Chief Technology Officer of Agility Communications, Inc. At UCSB, his efforts have included work on novel guided-wave and vertical-cavity modulators and lasers as well as the underlying materials growth and fabrication technology. He is now investigating the integration of various optoelectronic devices, including optical amplifiers and modulators, tunable lasers, wavelength converters, and surface-emitting lasers. He has authored or coauthored over 500 papers, five book chapters, and one textbook, and has been issued 32 patents.

Dr. Coldren is a Fellow of the Optical Society of America, a past Vice-President of the IEEE Lasers and Electro-Optics Society (LEOS), and has been active in technical meetings.